Dynamics of DNA Polymers in Post Arrays: Comparison of Single Molecule Experiments and Simulations

ARTICLE *in* MACROMOLECULES · APRIL 2007

Impact Factor: 5.8 · DOI: 10.1021/ma062892e

4 AUTHORS, INCLUDING:

Victor A. Beck
Palo Alto Research Center
9 PUBLICATIONS **72** CITATIONS

SEE PROFILE

Eric S. G. Shaqfeh
Stanford University
221 PUBLICATIONS **5,772** CITATIONS

SEE PROFILE

Dynamics of DNA Polymers in Post Arrays: Comparison of Single Molecule Experiments and Simulations

Nerayo P. Teclemariam,[†] Victor A. Beck,[‡] Eric S. G. Shaqfeh,[‡,§] and Susan J. Muller*[,†]

Department of Chemical Engineering, University of California, Berkeley, Berkeley, California 94720; Department of Chemical Engineering, Stanford University, Stanford, California 94305; and Department of Mechanical Engineering, Stanford University, Stanford, California 94305

Received December 18, 2006; Revised Manuscript Received March 8, 2007

ABSTRACT: Understanding the dynamics of biopolymers in complex flows is critical for the successful design of lab-on-a-chip devices. In this paper, we demonstrate the first direct comparison of experiments and simulations of DNA transport in a pressure-driven post array flow. High aspect ratio ordered silicon posts arrays were microfabricated, and single molecule experiments were employed to examine the dynamics of DNA traversing through arrays of ordered obstacles. Three different geometries with varying post spacing were tested, and probability distributions of DNA hooking location and fractional DNA lengths were generated. It is demonstrated that the appropriate design of post array geometry can be used to control DNA conformation and guide the location of hooking events. Finally, agreement between experimental and Brownian dynamics simulation results is good, validating the simulations that can be used to guide future array designs.

Introduction

The dynamics of DNA in flow has received considerable attention recently. Advances in both Brownian dynamics simulations and in direct visualization methods for individual DNA molecules have allowed detailed comparisons of experiments and computations in a range of simple shear, planar extensional, and linear mixed flows.[1−4] These studies have provided insights into DNA dynamics including molecular individualism,[5,6] the relaxation and transport of DNA in confined environments,[7−11] and conformational hysteresis in extensional flows.[2,3,12] These studies have also allowed the quantitative assessment of the ability of various bead−rod and bead−spring models of polymer chains to capture the actual chain dynamics.[4,13−18] While the dynamics of DNA in simple flows are now well understood, relatively few direct comparisons between simulations and experiments in more complex flows have been performed. In the present work, we focus on quantitative comparisons between bead−rod chain Brownian dynamics simulations and direct visualization experiments on DNA driven hydrodynamically through ordered arrays of microfabricated posts. This complex flow is of interest not only as a benchmark for simulation tools but also as a critical element in lab-on-a-chip devices designed to stretch and separate DNA for single molecule sequencing.[19] Hence, an important aspect of this work is the design of a device geometry and a flow to produce a specific conformation field.

Many researchers have studied the electrophoretic motion of DNA past single posts and post arrays. These studies were motivated in large part by the widespread use of gel electrophoresis for size-based separation of DNA; the DNA−post interactions serve as an idealized model of DNA interactions with the fixed obstacles provided by the gel matrix. The charged DNA chains are driven through a matrix of gel fibers by an applied electric field E; interactions with the obstacles (the gel fibers) cause the DNA chain mobility to be length dependent and hence provide a mechanism for separation. We briefly summarize these studies below; however, we note that there are important distinctions between electric and hydrodynamic fields. In addition, as detailed below, in many of these earlier studies accurate models for either the field and/or the DNA dynamics were not used.

Sevick and co-workers[20−22] were among the first to systematically simulate single post collisions and show a length-dependent DNA chain mobility. These authors considered single, point obstacles and modeled the DNA chain as a non-Brownian bead−spring chain. They demonstrated that for strong electric fields hooking of a DNA chain on the obstacle to form a hairpin configuration and the subsequent release of the DNA via a rope-over-a-pulley mechanism lead to a collision or trapping time that scales linearly with chain length N and inversely with electric field strength E. This strong stretching regime is characterized by PeN > 1, where the Peclet number, Pe, represents the ratio of convective to diffusive transport. For the electrophoretic motion considered, Pe is proportional to E. As discussed by Patel and Shaqfeh,[23] PeN can be interpreted as the ratio of chain relaxation time to hairpin formation time. Sevick and co-workers subsequently demonstrated that small offsets between the DNA center-of-mass and the post location were critical to hook formation[21] and that for finite-sized (conductive) posts a second chain release mechanism associated with "rolling off" the post after a glancing collision appears.[20] Obstacle radii R_{obs} from 0.75 to 15 times the DNA radius of gyration R_g were considered; this rolling-off mechanism becomes more likely than hooking for $R_{obs}/R_g > 1$ but does not result in significant extension of the chain and is independent of chain size. Andre and co-workers[24] considered the effects of hydrodynamic interactions on chain hooking in strong fields and found the effects negligible on fractionation via single collision processes.

Randall and Doyle[25−27] recently studied the electrophoretically driven collisions of DNA molecules with isolated (single), insulating posts. Fluorescence microscopy was used to directly visualize λ-DNA interacting with a post as a function of both

* Corresponding author: Tel (510) 642-4525; Fax (510) 642-4778; e-mail muller2@socrates.berkeley.edu.
[†] University of California, Berkeley.
[‡] Department of Chemical Engineering, Stanford University.
[§] Department of Mechanical Engineering, Stanford University.

10.1021/ma062892e CCC: $37.00
Published on Web 04/13/2007

the dimensionless offset b/R_g (where b is the distance between the impacting molecule's center-of-mass and the obstacle center) and obstacle size for $1.1 < R_{obs}/R_g < 15$ (corresponding to post radii of 0.8−10 μm). Both hooking and roll-off interactions were observed. In addition to offset and post size, these authors identified the importance of obstacle-induced electric field gradients, parametrized by a Deborah number De, in governing the hooking process. Brownian dynamics simulations, using a bead−spring chain consisting of 30 beads connected by worm-like springs, were also used to examine the impact dynamics at high De. Subsequently, they measured, classified, and modeled DNA hooking interactions with small, single posts; in addition to symmetric and asymmetric DNA hairpins that unhooked via the rope-over-a-pulley mechanism, they found a new, more probable "extending" collision in which the long arm of the hairpin continues unraveling during the unhooking process.[21]

Kenward and Slater, using molecular dynamics (MD) simulations, investigated both the collision of a polymer with a fixed molecular obstacle and the collision of a polymer with a second polymer when driven by an external force and by pluglike fluid flow.[28] Explicitly including a Lennard-Jones solvent and modeling obstacles as tightly packed columns of Lennard-Jones beads, the authors showed that polymer−obstacle collisions driven by an external force are qualitatively similar to those driven by fluid flow. However, the hydrodynamic coupling between the beads in the polymer when it is driven by fluid flow results in a key quantitative difference and leads to a reduced force on the obstacle. Furthermore, chain relaxation occurs during the final part of polymer−obstacle unhooking in external fields but is absent in fluid flow since the latter keeps the molecule elongated during the entire escape process.

Studies of DNA electrophoresis in post arrays have included simulations in dense, ordered arrays,[29,30] simulations in sparse, random arrays,[23] experiments in ordered 2D arrays,[31−33] and experiments in quasi-ordered arrays.[34−36] In some of the earliest studies, Deutsch and Madden[29,30] used Brownian dynamics simulations of bead−rod chains to model electrophoresis in dense, ordered post arrays. Using a lattice spacing of roughly twice the persistence length of DNA and obstacles with radii of roughly 0.4 persistence lengths, they qualitatively captured the experimental observations that in gels the mobility of chains saturates at relatively short chain lengths and increases monotonically with electric field strength.

Patel and Shaqfeh[23] subsequently used a similar approach to model electrophoresis in dilute periodic and disordered post arrays as a function of chain length, electric field strength, and array geometry. In these simulations, the diameter of the posts was one Kuhn length (~0.15 μm, a size achievable with electron beam lithography), and the DNA was constrained to two dimensions. Average chain velocities and streamwise dispersion coefficients were calculated for random arrays with post densities of 0.005 as a function of Pe and N. As expected, the motion of chains of all lengths is hindered by the obstacles, with the longest chains most hindered. Chain velocities display a minimum at moderate PeN, corresponding to a balance of chain relaxation and hairpin formation, and at high Pe dispersion leads to poor quality separations. In addition, Patel and Shaqfeh note that the agreement between simulations for random post arrays and single posts is limited to extremely dilute arrays due to the importance of chain relaxation. In ordered arrays with square and hexagonal post arrangements of the same density (0.005), chain velocities at high Pe were larger than in random arrays since the straight, open channels in ordered arrays reduce the collision frequency and hence hairpin formation. That is, in sparse ordered arrays, the collision frequency is controlled by the thermal diffusion of the chains, which scales as $(\mathrm{Pe}N)^{-1}$. At high Pe, chains in ordered arrays move at velocities near the free stream value, hairpin formation is rare, and separation is poor since the velocity is a very weak function of chain length.

The first experiments on DNA electrophoresis in ordered arrays were by Volkmuth and Austin.[31] They used optical microlithography to fabricate a regular, rectangular array of 0.15 μm high, 1.0 μm diameter posts with a center-to-center spacing of 2.0 μm. These short posts—roughly 2 persistence lengths in height—effectively confine DNA to two dimensions. Volkmuth and Austin used fluorescence microscopy to measure electrophoretic velocities in this array as a function of DNA length and found separation possible for DNA up to ~100 kb. More recently, Viovy and co-workers[34−36] have presented video microscopy studies of electrophoretic separation of DNA in arrays formed through the self-assembly of magnetic particles. These "Ephesia" arrays are nonregular and far sparser than those studied by Volkmuth. Quasi-periodic arrays of 12 μm tall obstacles with mean diameters from 0.95 to 1.74 μm and center-to-center distances from 3.4 to 13 μm, corresponding to array densities of 0.13 to 0.28, were fabricated. Fluorescence microscopy of T4 DNA (169 kbp, with a contour length of ~74 μm) was used to measure the number of collisions, collision duration, passage time through the viewing area, and the detailed trajectory in the field as a function of electric field strength. They find that the trapping time varies linearly with E^{-1} and is independent of the array density over the range considered, while the collision probability is observed to be independent of E and increases with post spacing (presumably due to relaxation). Their measurements of passage time allow them to estimate mean velocities and dispersivities, which show favorable agreement with a lattice Monte Carlo model.

A detailed comparison between the Brownian dynamics simulations and the experiments to date is difficult: the size of the fabricated posts in all the experiments is much larger than that simulated, and there are differences in the array spacing and geometry. For stained (5:1) λ-DNA, the contour length, persistence length, and radius of gyration are roughly 21 μm, 0.07 μm, and 0.7 μm, respectively, so Deutsch's simulations correspond to $R_{obs} \sim 0.03$ μm and a lattice spacing of 0.07 μm. Patel and Shaqfeh's simulated posts have $R_{obs} \sim 0.07$ μm, and their ordered arrays have a spacing of roughly 2 μm. Posts fabricated in the experiments described above have $R_{obs} \sim 0.5$ μm and a spacing of 2−13 μm.

Furthermore, while the above studies on electrophoretically driven motion of DNA in post arrays have provided considerable insight into size-based separation of DNA, the corresponding problem for hydrodynamically driven DNA has received little or no attention. There are significant differences between the two problems: in the case of hydrodynamic flows, the no slip boundary condition must be satisfied on all surfaces which is not true for the electrophoretic case. In addition, the rate at which disturbance fields decay with distance from the obstacles varies as r^{-3} for the electric field[37] and as r^{-1} for the hydrodynamic case in this low Reynolds number regime. Not all of the simulation studies above used accurate models of the DNA, and as noted, none used post sizes that can be easily obtained experimentally. Finally, the focus of nearly all the electrophoresis studies has been on understanding size-based separation; i.e., the mobility or velocity of the DNA through the array and its dependence on chain length, rather than on the ability of the array to stretch the DNA or the conformational statistics of the chain within the array, have been the key metrics reported.

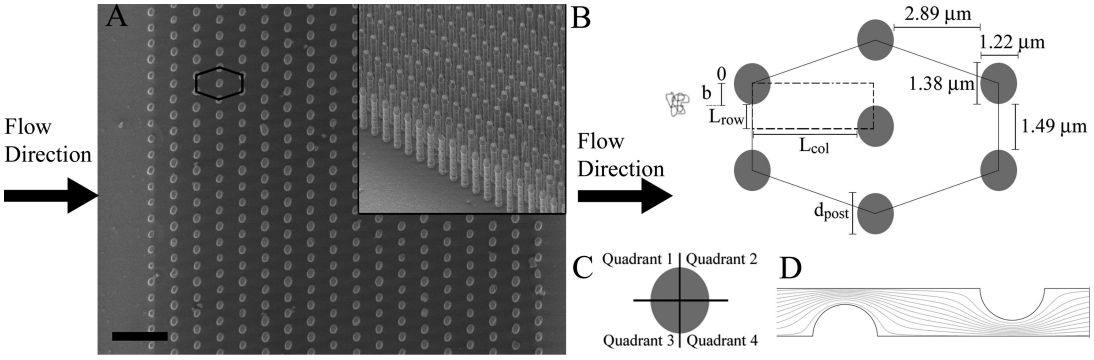

Figure 1. (A) Top and side view (inset) scanning electron micrographs of a typical post array used in the study. Scale bar is equal to 10 μm. (B) Schematic of stretched hexagonal geometry with dimensions, where d_{post} is the diameter of the post, L_{row} and L_{col} are respectively row and column post center-to-edge spacings of adjacent columns used for geometry optimization, and the dotted box indicates the partial unit cell used in the initial impact parameter analysis. (C) Schematic of four quadrants of a post used to define a hooking event. (D) Flow field streamlines through a typical post array used in simulations. Fluid flow direction is from left to right in all frames of the figure.

Here we report a quantitative comparison between experiments and simulations of hydrodynamically driven flow of DNA through ordered post arrays. High aspect ratio post arrays were fabricated using silicon microfabrication methods, and a pressure gradient was applied to drive the flow of dilute solutions of λ-DNA through the arrays. The motion of the DNA was visualized using fluorescence microscopy, and conformational statistics and hooking events were extracted as a function of initial offset (position of the DNA relative to the center of the first column of posts), position within the array, and flow strength (Pe). The array geometry was modeled on the basis of scanning electron micrographs of the array, and finite element simulations were performed to calculate the velocity field within the array. The velocity field and the measured experimental offsets were then used as inputs for Brownian dynamics simulations of Kramer's bead−rod chains of $N = 150$ beads (corresponding to λ-DNA) within the array.

Methods: Experiments and Simulations

Array Design and Parameter Definitions. Many array geometries have been used for single molecule studies of sequencing or separation in microfluidic environments including hexagonal,[31,32] square,[23] and random dilute arrays.[23,38] In this study a hexagonal array configuration was chosen as the model system due to its periodic nature and the resultant ease of calculation of the flow field for use in the Brownian dynamics simulations. High aspect ratio posts were desired to reduce top and bottom wall flow disturbances felt by the DNA molecules measured at the channel centerline. The channel height was designed to be large relative to the characteristic flow length scales within the array (post spacing or post diameter), so that the flow disturbances from the walls will not propagate significantly over a distance greater than the post spacing or diameter. This allowed the flow near the center of the channel to be approximated as a 2D flow. Initially, regular hexagonal arrays with equal row and column spacing were fabricated, tested experimentally, and compared to simulations. As anticipated by the work of Patel and Shaqfeh, this array geometry was found to yield a low number of hooked molecules,[39] as many molecules experienced channeling and were able to pass through open voids in the array without collision with a post. To generate a large number of hooks per molecule, one would like to repeatedly guide the trajectory of DNA molecules to lie near the center or stagnation streamline of posts. Within the array, because of the presence of low Reynolds' number laminar flow dictated by the micron-sized dimensions of the channel, the dominant method of transport for DNA across streamlines is via diffusion of the molecule.

A Peclet number, the ratio of convective to diffusive transport, was identified to gauge the relative importance of diffusion within the system and can be defined a number of ways; we have chosen the form

$$\mathrm{Pe} = \frac{\langle U \rangle d_{post}}{D_{DNA}} \tag{1}$$

where $\langle U \rangle$ is the average superficial velocity of DNA upstream of the array and d_{post} is the post diameter. Many characteristic lengths are present within the system, but the post diameter was chosen as it scales the flow perturbation felt by the DNA approaching the array. The diffusivity, D_{DNA}, was taken to be the value for λ-DNA measured by Chu et al.[40] in quiescent conditions and scaled linearly to account for the different solvent viscosity used in these studies.

The time to diffuse into the collision cross section of the next post is decreased by decreasing the row spacing L_{row} (cf. Figure 1), which reduces the distance a DNA molecule that failed to hook or experienced a nonhooking roll-off must diffuse to lie near the stagnation streamline of the next downstream post. In addition, increasing the column spacing L_{col} will allow the molecules more time to diffuse between columns of posts. In fact, the geometry that optimizes collisions based on these considerations depends on the characteristic velocity $\langle U \rangle$ in the array (or equivalently, the Peclet number). A simple scaling argument suggests that maximum hooking will occur when

$$\frac{\langle U \rangle}{D_{DNA}} \leq \frac{2L_{col}}{L_{row}^{\,2}} \tag{2}$$

where D_{DNA} is the diffusivity of λ-DNA. In the present experiments and simulations, these improvements (reduced row spacing and increased column spacing) were incorporated into the array design to yield geometries with stretched hexagonal configurations (cf. Figure 1). We have defined a parameter we call the overlap percentage as

$$\text{overlap } \% = \frac{d_{post} - 2L_{row}}{d_{post}} \times 100 \tag{3}$$

that quantifies the apparent overlap of posts when viewed along the flow direction. Negative values of the overlap percentage thus correspond to arrays with open channels in the flow direction. It should be noted that we have not optimized the arrays for each characteristic velocity or Peclet number; rather we have used a consistent range of Pe for all the array experiments to facilitate comparison.

An important parameter in determining hooking in previous single post studies is the impact parameter defined as

$$\beta = \frac{b}{R_g} \tag{4}$$

where b is the distance perpendicular to the flow between the center-of-mass of a DNA molecule entering the array and the post center. R_g is the equilibrium radius of gyration of λ-DNA, taken from the literature for stained λ-DNA to be 0.7 μm.[40] As noted in the Introduction, previous single post studies have shown that when β is small, DNA molecules lie near the stagnation streamline of posts and experience a high probability of hooking.[25] These single post impact parameters can be extended to array geometries by looking at a portion of the unit cell and taking the initial position, b, with respect to the first column of posts (cf. Figure 1).

Materials. Double-stranded bacteriophage λ-DNA (48.5 kb, New England Biolabs) was chosen as the model biological macromolecule for these experiments, as it has been well-characterized within the literature and has been shown to follow the wormlike chain force law.[41] YOYO-1 (Molecular Probes), a dimeric cyanine fluorescent dye, was used to label λ-DNA and has been reported to increase the persistence length by 37% at the dye concentration (5:1) used in these experiments,[42] yielding a contour length of 21 μm. As per other researchers, the DNA solutions contained a solvent mixture of 10 mM Tris buffer pH 8.0, 10 mM NaCl, 1 mM EDTA and 44.8% (w/w) sucrose; labeling with YOYO-1 proceeded as described in ref 12. At the percentage of sucrose used here, the DNA solution viscosity was 9.2 cP, measured with a Vilastic-3 Viscoelasticity analyzer (Vilastic) at 25 °C. To retard photobleaching, an oxygen scavenging mixture of glucose (0.0001 mg/mL), glucose oxidase (0.005 mg/mL), catalase (0.001 mg/mL), and β-mercaptoethanol (4% v/v) was added to the solvent. All incubations and experiments were performed in a dark room. The longest relaxation time of λ-DNA was determined by measuring the apparent length of DNA molecules after release from hooking events on the last two rows of the array and fitting the final portion of the relaxation ($x/L < 0.3$) to the following equation:

$$\langle x(t)\, x(t)\rangle = a \exp(-t/\tau) + b \tag{5}$$

The longest relaxation time was measured to be $\tau = 1.04 \pm 0.16$ s, close to the scaled (due to viscosity differences) experimentally reported value of $\tau = 0.84$.[42,43]

Device Fabrication. Standard microelectromechanical system (MEMS) silicon fabrication was chosen to produce the post arrays and microfluidic system. This was chosen over soft lithography because of its ability to create high-aspect ratio structures, the ease of compatibility with other possible components (e.g., integrated microheaters), and the dimensional stability, lack of compliance, and absence of fluid permeation of the resultant devices. In contrast, soft lithography typically employs polydimethylsiloxane (PDMS) and is limited to aspect ratios (height/length) of 0.2−2 for defect free devices;[43] in addition, devices may deform under an applied pressure and permeation flows may become important.[44] In the present studies, post diameters ~1 μm in diameter were desired, which limits the height of posts produced using soft lithography to just 2 μm. At this height, confinement effects and hydrodynamic interactions between the DNA and channel walls have been shown to significantly alter the relaxation and persistence lengths of DNA,[7,8] and the flow field throughout the device is not well approximated as two-dimensional.

Using standard optical lithography and deep reactive ion etching (DRIE) utilizing the Bosch process, a series of post arrays were fabricated. Scanning electron micrographs of a typical array are shown in Figure 1A; here 1.22 μm × 1.38 μm (length × width) posts, 14.2 μm in height, were fabricated in a channel 300 μm wide and 14.2 μm deep. The overall length of the flow channel was 17.5 mm, and the posts were placed 3.25 mm downstream of the channel entrance to ensure fully developed flow upstream of the post array. The asymmetry of the posts is due to imperfections in the photolithography mask and variability of processing conditions (e.g., exposure lamp intensity and photoresist development time) and the fact that the fabrication methods used in this study are being pushed beyond the 2 μm resolution limit of traditional optical lithography. The dimensions of other arrays used in this study are summarized in Table 1, where $d_{transverse}$ and $d_{parallel}$ are the post diameters measured perpendicular and parallel to the flow direction, respectively.

Table 1. Summary of Post Array Geometries and Field Strengths Probed[a]

% overlap	$d_{transverse}$ (μm)	$d_{parallel}$ (μm)	no. of columns	Peclet numbers
−80	1.50	1.86	10	353, 731, 834, 1604
−8	1.38	1.22	18	262, 436, 1285, 1706
37	1.79	1.78	18	699, 1242

[a] The quantities $d_{transverse}$ and $d_{parallel}$ are the post diameters measured perpendicular and parallel to the flow direction, respectively.

For each array, anodic bonding of a 170 μm thick, piranha-cleaned glass coverslip to the silicon device at 450 °C and 1000 V for 1 h sealed the channels. A diamond bit (S40MD, Amplex Abrasives) was used to drill holes at the extreme ends of the device for out-of-plane interconnections for flow inlet and outlet. Cut luer tips (Cole-Parmer) were attached to the backside of the devices using epoxy, and 1/16 in. Tygon tubing (Cole-Parmer) connected the devices to the flow source. Because of compliance issues (expansion of tubing walls due to applied pressure), the system was allowed to equilibrate for at least 20 min before measurements were taken. Furthermore, the superficial velocities of individual DNA molecules measured at the centerline (depth) of the channel, away from sidewalls, and upstream of the post arrays were compared before, during, and after the experiments to confirm the existence of a stable flow rate.

Flow Apparatus. Two methods of generating flow were employed in the experiments. For relatively high flow rates (>1 μL/h) a syringe pump (Cole-Parmer 74900 series) was used. For low flow rates, hydrostatic pressure was used, which provided more stable flow rates than the syringe pump. The upper limit of flow rate was determined by the image capture rate and the onset of optical streaking; in practice, this was determined by imaging 0.7 μm microbeads (Polysciences, Inc.) at various flow rates. The lower limit of flow rate was set to allow a molecule to traverse the entire experimental field of view within the image capture system's memory. Using the above methods, we were able to achieve flow rates, Q, and Peclet numbers within the range of 0.14 μL/h < Q < 1.5 μL/h and 262 < Pe < 2800 for the channel sizes tested in these experiments.

An inverted epifluorescence microscope (Leica DMIRE2) with a 50 W high-pressure mercury lamp, 100×/1.4NA oil immersion objective (Leica HCX PL APO), excitation 450-490 nm and emission long pass 515 nm filters, and a CCD camera was used to visualize the flow of YOYO-labeled DNA. Two cameras were employed: a high-performance monochrome Cohu 4900 series and CASCADE 512BFT (Roper Scientific) CCD camera. In the case of the Cohu camera, the images of the DNA were captured and amplified with a high-gain image intensifier (KS-1381 Videoscope International Ltd.), transferred to PC via a framegrabber, and analyzed using the software NIH IMAGE. Images captured with the CASCADE 512BFT were captured as 16-bit images to PC using SimplePCI and ACI image software (Compix, Inc). In both cases, images were converted to 8-bit (0−255 gray scales), and the background intensity was subtracted using macros written in NIH IMAGE software. Programs shifting the baseline pixel intensity value and stretching the intensity distributions were written and used to process images, increasing clarity and reducing noise of the images.

Imaging and Conformation Analysis. A mouse-controlled cursor was used to measure DNA positions and apparent lengths within the array from the captured images. Reported lengths are the largest distance between opposite ends of the DNA molecule, typically oriented in the flow direction. Because of the fact that DNA molecules continually fluctuate in and out of focus during hooking, molecules were measured by hand. This method, which has also been used by other researchers,[35] provided accurate results but is extremely labor intensive leading to limited ensembles sizes. Ensembles of at least 100 molecules were measured at each flow

strength (Pe) and post configuration to attempt to provide sufficient statistics to accurately quantify the effect of the different experimental parameters. A hooking event was defined when a DNA molecule engaged a post and segments of the same molecule were simultaneously present in all four quadrants of a post (cf. Figure 1C).

Simulation Method. The Brownian dynamics (BD) simulation technique has been used to model polymeric molecules in a variety of situations including the simulation of chain−obstacle dynamics.[20,23] Patel and Shaqfeh previously employed BD to study the dynamics of chains in both ordered and random arrays of conducting, Kuhn-step sized obstacles. In this work, the same technique is extended to model chain dynamics through ordered arrays of larger posts while accounting for the effects of field disturbances due to the presence of the posts.

As in previous work, fluorescently tagged λ-DNA is modeled using the Kramers freely jointed bead−rod chain model.[45,46] This model has demonstrated quantitative agreement with experiments in single molecule flow studies of DNA even though the model does not reproduce the correct bending forces or effective entropic spring force of the wormlike chain or Kratky−Porod model.[47,48] To simulate the Kratky−Porod model, however, in the present application, ~10 sub-Kuhn step level discretization points are needed in order to produce the correct persistence length in a discrete model appropriate for Brownian dynamics.[49] Thus, the number of dynamics variables becomes prohibitively large for the long time, large ensemble simulations considered in this work (see Ensemble Size section below). Therefore, we choose to focus on the qualitative comparisons to the experimental data with our simulations. As we shall discuss below, errors associated with ensemble size in these comparisons are at least as important as those associated with the shortcomings of the model.

In the Kramers model, the polyelectrolyte is divided into N beads, at which the mass and hydrodynamic drag are concentrated, connected by $N - 1$ massless rods. The entire molecule has a contour length of ~21 μm and is modeled using 150 beads, yielding a Kuhn step size, b_k, of 0.142 μm.[40] The drag is assumed to be isotropic, and hydrodynamic interactions (HI) between segments of the chain are ignored. Experiments and simulations performed on λ-DNA in viscous, extensional flow[2,3] have shown that, due to the expanded configuration of the chain, HI has little effect on the dynamics of the chain; of course, HI would become increasingly important for longer chains. HI could influence the dynamics of a λ-DNA chain unwinding around a post if there are multiple folds. However, computer simulations have shown that the latter phenomenon has no significant quantitative or qualitative effects on chain dynamics.[24] Hence, the polyelectrolytes in these simulations are modeled as freely draining chains.

As detailed in previous work,[45,50] the Langevin description serves as the starting point for the development of the model. Assuming the bead mass is negligible, the sum of the Brownian, hydrodynamic, constraint, and excluded volume forces on bead α is

$$F_i^{\mathrm{Br},\alpha} + F_i^{\mathrm{Hyd},\alpha} + F_i^{\mathrm{C},\alpha} + F_i^{\mathrm{EV},\alpha} = 0 \tag{6}$$

The Brownian forces are random and can be approximated as an uncorrelated white noise. These are determined by appealing to the fluctuation−dissipation theorem[51]

$$\langle F_i^{\mathrm{Br},\alpha}(t)\rangle = 0 \tag{7}$$

$$\langle F_i^{\mathrm{Br},\alpha}(t), F_j^{\mathrm{Br},\beta}(t')\rangle = 2kT\varsigma\delta_{ij}\delta_{\alpha\beta}\delta(t - t') \tag{8}$$

In (8) ζ is the drag coefficient for a bead, kT the thermal energy, and δ the Kronecker or Dirac delta. The excluded volume force between the post and the chain is determined as in previous work by taking the repulsive part of the Lennard-Jones potential.[23] The constraint forces are tensions along the rods in the chain and serve to rigidly link the beads a distance b_k apart. These tensions are determined iteratively and are the principal step in the integration of the evolution equation.[45,50,52]

The remaining term in the Langevin equation is the hydrodynamic force. For a freely draining chain, the hydrodynamic force on a bead is

$$F_i^{\mathrm{Hyd},\alpha} = -\varsigma(\dot{r}_i^{\alpha} - u_i^{\infty}(r_i^{\alpha})) \tag{9}$$

where r_i^{α} is the position of the bead and the overdot represents a time derivative. The flow field is given by u_i^{∞} and is undisturbed by the presence of the bead−rod chain.

In this work we are concerned with the viscous flow of bead−rod chains through ordered arrays of posts. There is no simple analytic formulation for the ambient flow field, and we determine it numerically. To facilitate comparison to the experiments, the post array geometry is chosen to match the geometry of the experimentally fabricated posts. Thus, we use a commercial finite element solver (COMSOL) to solve for the two-dimensional flow field in these arrays in the limit of negligible fluid inertia (i.e., the limit of zero Reynold's number, $\mathrm{Re} \to 0$). Elements were of sub-Kuhn step length and varied slightly with post diameter, with the typical element size being of order 0.05 Kuhn steps. This allowed the flow field to be resolved at a finer grain than the dynamics of the bead−rod chains. A typical post array geometry used for flow field generation is featured with streamlines as Figure 1D. Mesh convergence was verified by evaluating conservation of mass in and out of the array and by point-by-point velocity comparisons at various mesh resolutions. The numerical solution for the velocity field is then linked to our Brownian dynamics simulations through (9) using a linear interpolation scheme for the velocity.

We nondimensionalize distance with b_k, force with kT/b_k, and time with the bead diffusion time $\zeta b_k^2/kT$. This yields the Peclet number, $\mathrm{Pe}_{\mathrm{sim}} = U\zeta b_k/kT$, with U the imposed superficial velocity far upstream of the posts, as the principal parameter governing the dynamics in our simulations. This Peclet number is the ratio of the time needed for the bead to diffuse a distance b_k to the time necessary for the flow to convect a bead the same distance. In these simulations, $\mathrm{Pe}_{\mathrm{sim}}$ serves to control the relative importance of Brownian motion. Results below, however, are reported in terms of the Peclet number Pe defined in eq 1.

Individual chain simulations were performed by first allowing chains to relax for several thousand dimensionless time units to an equilibrium configuration. In the experiments, the lengths of the chains are measured directly upstream from the beginning of the post array. These lengths were used to determine the initial stretch of the chains in our simulations. After relaxing a chain in the simulations to an equilibrium coil, the chain was pre-extended using an extensional flow at a Deborah number (given as the product of the relaxation time and the strain rate) of 35.5, until its length corresponded to the extension of a DNA chain in the experiment. This transient extension was repeated for each chain in the simulation ensemble. The magnitude of the Deborah number was chosen to exceed that required for the coil−stretch transition of a polymer in extensional flow ($\mathrm{De} = 0.5$) in order to rapidly stretch the chains. A shearing flow could have also been used to prestretch molecules; however, molecular individualism ensures that for chains not highly extended ($x/L < 0.3$) configurations will be highly variable and nearly indistinguishable from those generated by preshearing.[5,6] Moreover, simulated chains are placed ~20 Kuhn steps in front of the post array and undergo a number of time step evolutions (dependent on Pe) before they collide with a post, which effectively erases memory of the initial conformation. Therefore, chains prestretched to the relatively small extensions observed in the experiments using extensional flow will have an initial configuration that would compare well to a chain stretched in a shearing flow.

Furthermore, we chose as the starting offset position of the chain the corresponding experimentally measured offset. The chain simulation was then performed from this initial condition, through the array, until the chain passed by as many columns of posts as in

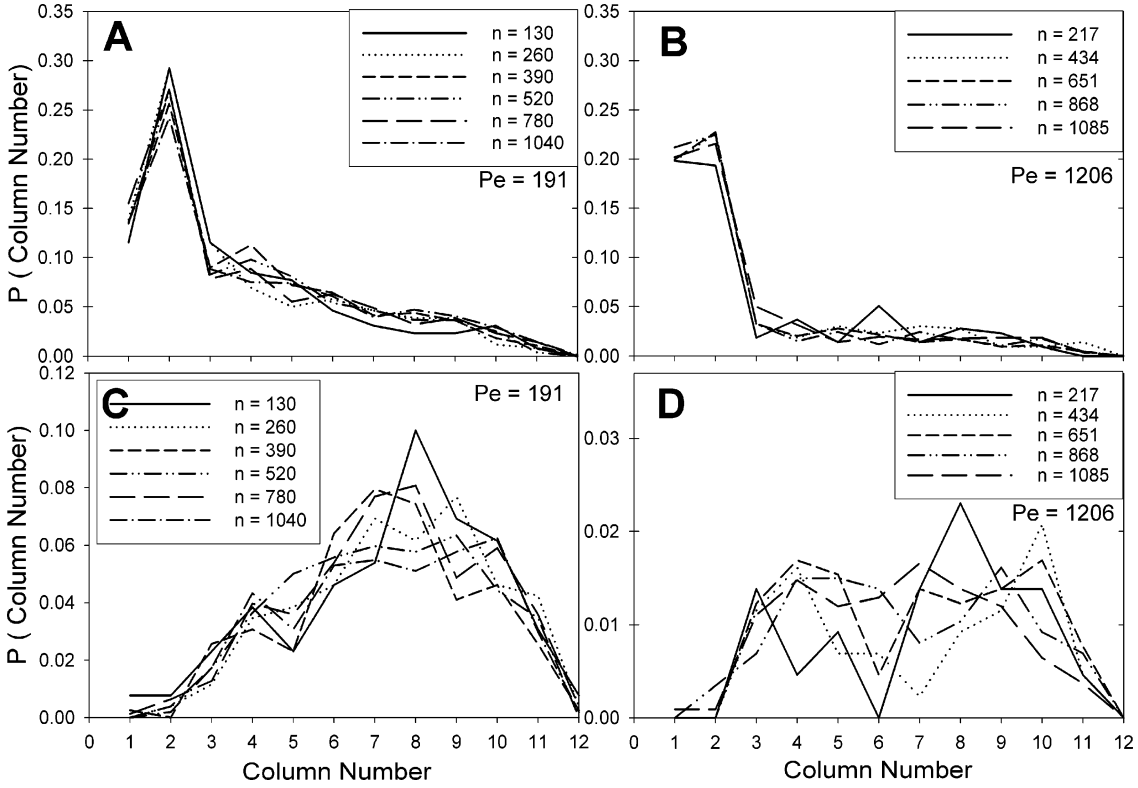

Figure 2. Simulation ensemble size studies showing convergence of probability distributions of hooking location for first and second hooks in a −37% overlap array. The number of molecules in the ensemble is *n*. (A) First hook distribution at Pe = 191. (B) First hook distribution at Pe = 1206. (C) Second hook distribution at Pe = 191. (D) Second hook distribution at Pe = 1206.

the experiments. As implied by the correspondence between the experimental and simulation initial conditions, these simulations were initially performed for the same size ensembles as the experiments, 100−200 molecules. As will be discussed in further detail below, larger ensembles are needed for convergence. These were obtained by running multiple simulations of the smaller experimental ensembles, using the experimentally determined initial lengths and offsets, but varying the initial configuration and random number sequence (Brownian motion). This technique allowed ensembles as large as 1300 molecules to be achieved in the simulations. In the following sections, results from experiments are compared to simulations based on a minimum of 1000 chains.

Results and Discussion

Ensemble Size. Single molecule experiments offer tremendous insight into the individual dynamics of molecules; however, relating these results to bulk averages requires the appropriate choice of ensemble size. To study the effects of ensemble size on the quality of the measured statistics in our complex flow geometry, we performed simulations of 130−1255 molecule ensembles in an array with −37% overlap. Large simulation ensemble sizes were created by repeated running of smaller simulations, each having the identical initial offsets and initial lengths specified by the experimental ensembles of size 100−200 molecules. These small ensembles were run with identical conditions, except the initial chain configuration and random number sequence (Brownian motion) was varied for each simulation. For example, a 390-chain ensemble was achieved by running a 130-chain ensemble three separate times using different random number sequences and initial chain configurations, but the same experimentally determined initial offsets and lengths. In Figure 2, we present probability distributions of first and second hooking locations within the array at two Peclet numbers. Analysis of the two sets of graphs shows that a smaller number of molecules is needed to see a convergence of second hooks at low Pelect number relative to high Peclet number; at Pe = 1206, roughly 500−1000 molecules are needed (cf. Figure 2D). However, as little as 100 molecules are needed at low Pe to capture the apparent shape of the large ensemble distribution. Interestingly, examining the distributions of first hook location shows almost identical results at all chosen ensemble sizes. We theorize that the location of the first hook is mainly determined by the array geometry and the inlet impact parameter. Unlike the middle of the array where the distribution of second hooking locations is maximum, the flow field around the first two columns of the array is not influenced by upstream posts; rather, the flow field is relatively uniform. In addition, over the range of Pe studied, the DNA is coiled upon entering the array with multiple streamlines passing through a molecule, each having different trajectories around a post. These effects lead to the importance of the DNA molecule's inlet impact parameter, chain configuration, and the array geometry on first hooks. In contrast, after hooking a stretched molecule has a small collision cross section and is more likely to follow a streamline around a post until it relaxes; hence, second hooks are much more sensitive to Pe.

Differences in sizes of ensembles necessary for convergence across the range of Pe investigated are hypothesized to be weakly influenced by any variation in the preimpact stretching of molecules caused by the extensional flow present upstream of a post. Over the range of flow rates of this study, the relative strain rates immediately before the post are of sufficient magnitude to deform the polymer, but the overall strains imparted on the molecules are relatively low due to the small time each molecule is present in this field. Therefore, we expect and observe experimentally negligible prestretching of molecules immediately before collision. However, the state of the polymer after collision measured as apparent length and the average velocity in the array do vary with Pe. The larger Peclet number

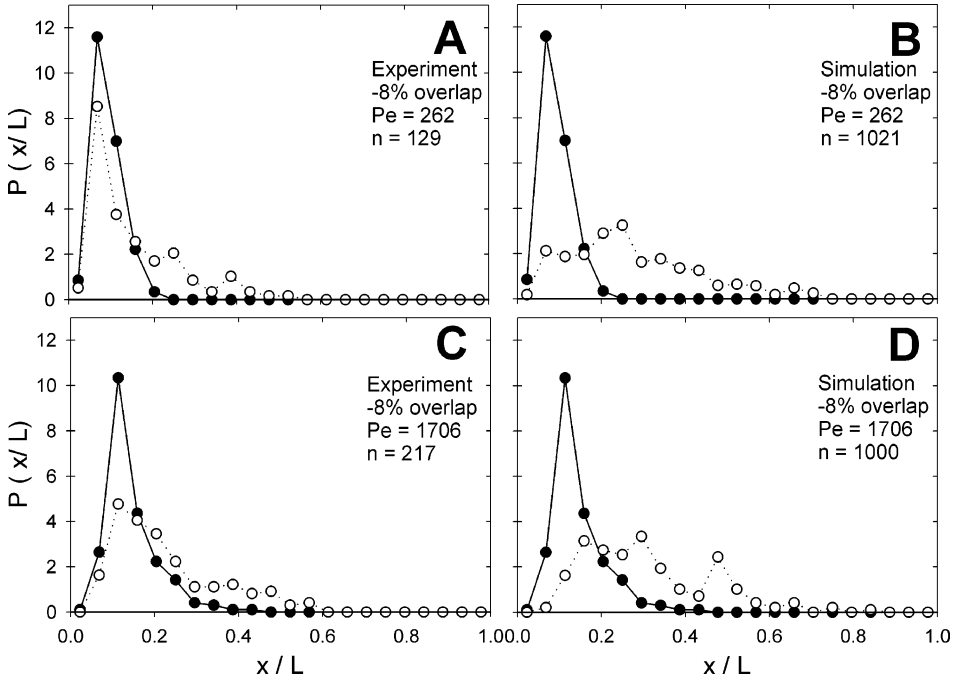

Figure 3. Experimental and simulation probability distributions of fractional lengths in −8% overlap array measured before and just upstream of the 13th column of posts in an 18-column array at various Peclet numbers. (A) Experiment, Pe = 262. (B) Simulation, Pe = 262. (C) Experiment, Pe = 1706. (D) Simulation, Pe = 1706. Filled circles are upstream of the array; open circles are when DNA reaches the 12th column. The number of molecules in the ensemble is *n*.

flow provides an increased viscous force on the arms of a hooked molecule, leading to more extended molecules upon release.[27] In addition, the decreased average velocity in the array at low Pe results in a 6-fold increase in traveling time for a given distance with respect to the high Pe case, allowing the molecules more time to relax back to their initial configuration. These combined effects lead to a larger collision cross section for the lower Pe number data set, which will have a higher probability of interacting and hooking with a post. Moreover, the high Pe data set appears to be very sensitive to the initial conformation of the molecule. High field strengths stretch chains, confining them to a narrow region of streamlines, and allow less time for the molecule to sample conformational space before colliding into a post.

As discussed in the Materials section, data analysis of movies captured in this study proved to be very labor- and time-intensive, limiting our experimental ensemble sizes to 100−250 molecules. The simulations presented in Figure 2 indicate that our experiments will at a minimum capture the qualitative shape of the distributions and should be more than sufficient at low Pe to analyze the effects of geometry on stretching and hooking of λ-DNA in our microfabricated arrays. At high Pe, simulations suggest that much larger ensembles may be needed to fully quantitatively capture the complex dynamics within the array; these larger experimental ensembles were not accessible in the present study.

Extension Probability Distributions. As one potential application of microfabricated post arrays is the controlled stretching of biopolymers, we begin by determining the effectiveness of the array for stretching. Probability distributions of fractional DNA extension before the array and after the leading end of nonhooked DNA traveled past the 12th column of an 18-column array are presented in Figure 3 for experiments and simulations at Pe = 262 and 1706. Experimental ensembles of greater than 100 molecules were acquired and a minimum of 1000 chains were run in the matching simulations. The "before" position is 1.5 post diameters upstream of the first column of posts; the "after" position was just upstream of the 13th column of posts. Our experimental field of view at the magnification chosen in these experiments allowed viewing of only about 13 columns of the total array. Upstream of the array, some fraction of molecules are extended slightly beyond their quiescent equilibrium extension ($x/L = 0.08$) due to the presence of Poiseuille flow within the channel; however, the majority are still in a compact globular configuration. A Weissenberg number based on in-plane flow gradients upstream of the post array was found to vary from 1.8 to 8 over the range of flow rates used in this study. After traveling past ~12 columns within the array, the distribution broadens and a tail develops at higher fractional extensions caused by the hooking and stretching of molecules around posts. A significant portion of the population appears to experience only slight extension after traveling through multiple columns in the array, and at first glance it might seem that a majority of molecules traverse the array without undergoing a single hooking event, the major cause of extension in the array. However, this is not the case as 72% of all molecules in the experiments and 95% in simulations were found to form at least one hook within the array at Pe = 262.

Additional distributions, not shown, at Pe = 436, 1285, and 1706 yield similar shifts in extensions after passing through 12 columns in the arrays. We note that the initial length distributions broaden as the Peclet number is increased, caused by the increase in upstream channel shear rate. This slight prestretching of DNA molecules reduces the collision cross section available for hooking and could be a factor in the observed reduction in the number of molecules that formed at least one hook in the simulations. Our Brownian dynamics simulations, like the experiments, show a shift in the length distributions toward higher fractional extensions after 12 columns in the array; however, molecules in the simulations are slightly more elongated than those in the experiments. Differences between the fractional length distributions in experiments and simulations are discussed below.

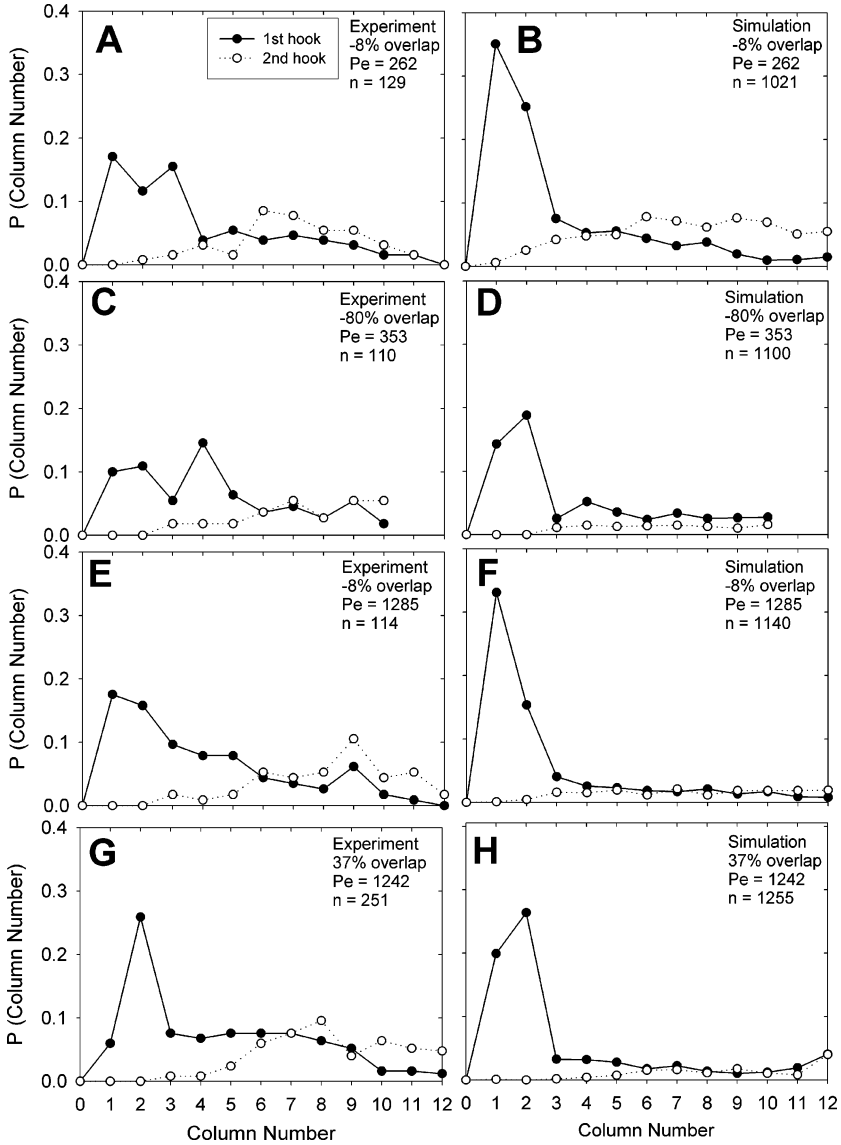

Figure 4. Experiments and simulations of first and second hooking location probability distributions at various overlap (−80%, −8%, 37%) and Pe. Closed circles and solid lines indicate distribution of first hooks, and open circles with dotted lines are for second hooks.

Hooking Probability Distributions. While the qualitative agreement between experiments and simulations with respect to the probability distributions of extensions are encouraging, a closer examination of the locations of hooks within the array provides insight into the underlying physics of the system. Inspection of both the experimental and simulation movies shows the complex motion of the DNA molecules through the array. As noted by other researchers,[29,35,53] a cyclical pattern of DNA motion is present which can be broken down into three distinct parts: (i) DNA collision with a post and hook formation, (ii) extension in the flow field and release with a rope-over-pulley or extended mechanism, and (iii) relaxation toward its equilibrium configuration and collision with another post at some downstream distance.

In our experimental field of view for each movie, up to three hooking events per molecule are observed in both experiments and simulations. The location and column number of each DNA molecule's first and second hook were recorded, and a probability distribution was created. Figure 4A−H shows the probability of hooking as a function of column number within the first 12 columns for three different overlap geometries and varying Pe. Analysis shows the presence of multiple peaks in the probability of first and second hooks at distinct column locations within the array. At Pe = 262 and −8% overlap the peak in the probability of first hooks occurs around the second column, and the peak in probability of second hooks is approximately the sixth column.

We can examine the effect of Pe on the distribution by looking at the −8% overlap geometry at Pe = 262 and 1242 (Figure 4, A and E). A slight broadening of the first hooking distribution is noted as Pe is increased; however, the most striking difference is in the second hooking location distribution, which experiences a shift toward later columns. We expect that as the Pe is increased the ratio of chain relaxation to characteristic convective time, inversely proportional to velocity, increases and DNA molecules have less time to relax for a given distance. Molecules must then travel farther in the array to relax back to a critical collision cross section where they have a higher probability of interacting with a post. The shift in second hooks is also seen experimentally in the two other geometries tested (data not shown).

Comparing parts A and C of Figure 4, we can examine the effect of overlap as the geometry is changed from −8% to −80% overlap, effectively increasing the gap between rows and moving from an array where the posts in adjacent columns almost overlap to a more sparse array. The prominent peak in

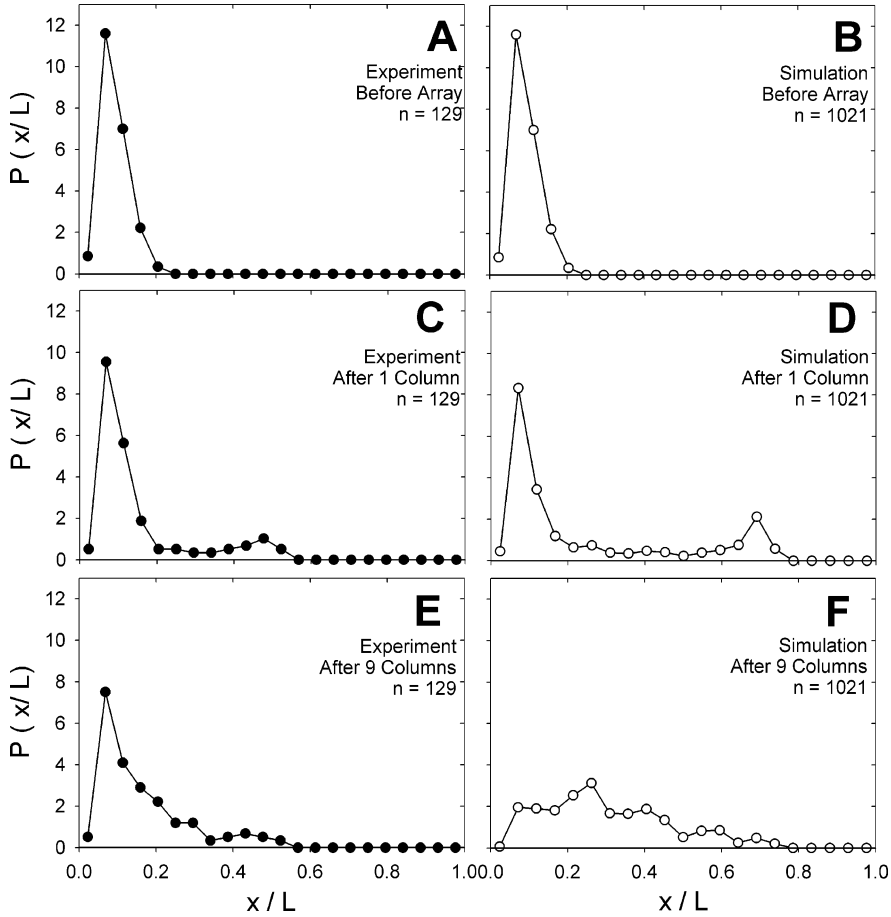

Figure 5. Experimental (A, C, E) and simulation (B, D, F) probability distributions of DNA fractional length at several locations within an array and Pe = 262. The number of molecules in the ensemble is *n*.

the first hook location distribution decreases and broadens as the overlap decreases. In addition, the peak in second hooks flattens. Inspection of the movies suggests that the decrease in second hooks is caused by channeling of the DNA after release from its first hook. Comparison of parts E and G of Figure 4 shows the effect of increasing overlap from −8% to 37%. As the overlap is increased, the probability of hooking on column two increases; however, the probability at column one decreases. The maximum in the second hook location distribution shifts to earlier within the array.

The Brownian dynamics simulations capture the high probability of hook formation within the first three columns of posts, the broad shape of the distributions, and maxima in second hooks in some cases. The dependence of the hooking location distributions on Pe and overlap in simulations is roughly consistent with experiments, with better agreement achieved at lower Pe as we would expect from our ensemble study. Differences in the hooking distributions may be due to the different initial configurations of the polymer chains, or molecular individualism, that provide a molecule with a unique hooking and unraveling experience. We have observed this in both experiments and simulations by watching chains of the same apparent length and initial offset interact differently with a post. Although the experimentally measured DNA lengths at the entrance of the array were used as an input for the simulations, the initial conformations could not be resolved using fluorescence microscopy. Thus, there are inevitable differences between the initial DNA conformation in the experiments and simulations. However, the agreement between the experiments and simulations with respect to hooking location suggests that the velocity field, initial offset parameter, and diffusivity of the DNA are sufficient to at least qualitatively describe the hooking dynamics via simulations.

For engineering lab-on-a-chip applications the hooking location distributions above are especially interesting, because they suggest that only two or three columns are needed to generate a hook and stretch biopolymers. The presence of fewer columns in a design is advantageous as it reduces the flow resistance present in the channels and lowers the magnitude of pressure required to drive the flow. In addition, increasing the overlap percentage and decreasing the Pe was shown to shift the second hook location distribution toward the beginning of the array, which could be used to tailor biopolymer separation systems.

Extension Distributions within the Array. To further investigate the dynamical hooking, stretching, and relaxation of DNA molecules within the array, probability distributions of DNA fractional length were measured at various positions within the array (cf. Figure 5) at Pe = 262. As stated previously, DNA molecules enter the array very near their coiled equilibrium state, and after passing through the first column of posts a significant fraction of the population experiences a hooking event. These hooked molecules stretch out in the viscous flow and give rise to a bimodal fractional length distribution. This result is captured in both the experiments and Brownian dynamics simulations (Figure 5C,D), although the degree of extension is greater in the simulations. After nine columns within the array the bimodal distribution collapses as the majority of DNA molecules relax after experiencing a second hooking event near the sixth column. Again, the simulations capture the qualitative nature of the distributions measured experimentally with a slight shift toward higher extensions. It should be noted that the extensional flow present in the gap between the posts

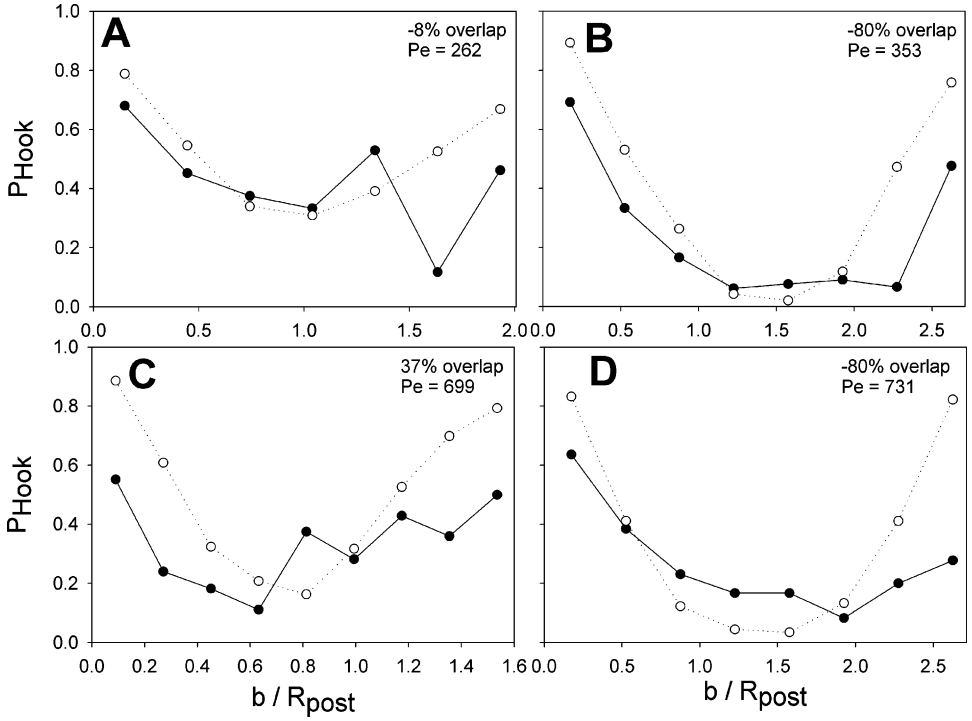

Figure 6. Experimental and simulation results for probability of forming a hook after second column (simulations) and third column (experiments) vs initial impact parameter at various overlap percentage and Pe. Closed circles and solid lines indicate distribution of experiments and open circles with dotted lines are simulations. The number of molecules captured in experiment are (A)−(D) 130, 110, 243, and 119. The number of chains run in simulations are (A)−(D) 1000, 1100, 1215, and 1190.

was observed to stretch DNA molecules; however, this effect was small relative to the extensions caused by hooking.

Quantitative differences between the simulations and experiments are theorized to be due in large part to the differences in experimental and simulation chain force-laws. λ-DNA is known to follow the wormlike chain force law (WLC) while Kramer's bead rod models have an inverse Langevin relationship (IL).[41] Quantitatively, these force laws converge at fractional extensions less than 0.3, but at higher extensions the IL force law softens and yields larger extensions for a given force compared to the WLC model. Evaluating a typical experimental fractional length of 0.6 shows that the IL force law predicts a length of 0.72, which is consistent with the overpredicted extensions in our simulations.

Effect of Impact Parameter on Probability of Hooking and Extension. We investigated the importance of the initial impact parameter on the probability of hooking, which to date has been examined only in single post studies. Defining a portion of the unit cell (cf. Figure 1B), we determined the inlet offset of the DNA molecules to one pixel camera resolution. A probability of hooking distribution can be calculated by counting the number of DNA molecules that hook in a particular bin of inlet offsets and dividing by the total number of molecules within that same bin. As we are determining the probability of first hooking events within the start of the array, and Figure 4A shows that the experimental first hooking distribution is slightly broader than the simulations, we have chosen to calculate the experimental probability of hooking after three columns. Plotting the probability of hooking vs initial impact parameter for our three overlap percentages (cf. Figure 6) supports the observations of single post studies[21,26] that DNA molecules positioned near the center (or stagnation streamline) of a post have the highest probability of hook formation. The plot also shows that molecules initially aligned near the edges of the posts can still undergo hooking, although most such molecules avoid the posts or experience glancing collisions, verified in our movies. Comparison of parts A and B of Figure 6 shows the drastic drop in hooking probability as the overlap percentage is decreased and molecules have more space to travel between posts. The effects of Pe, at least over the range examined, are modest (cf. Figure 6B,D). The simulations and experiment agree fairly well. The main source of error is in the accuracy of the experimentally determined offset. In order to maximize the resolution of our probability of hooking plots, a one pixel bin size was chosen; however, this causes the slightest of experimental errors to greatly influence the data.

Trapping Times. In addition to quantifying the hooking location and stretching of DNA molecules, the trapping time, defined as the duration of time between the initial engagement of a hooking molecule on a post and its complete release, was measured. Ensembles were acquired and the mean trapping time was plotted vs 1/Pe in Figure 7. It has been shown in the literature both experimentally and via molecular dynamics (MD) simulations and a generalized collision model that in the high field limit the trapping time scales as the inverse field strength.[28,35] In our experiments, the Peclet number is proportional to the upstream velocity (field strength); therefore, a 1/Pe dependence is expected and observed. Both our experiments and simulations show a linear dependence of trapping time on 1/Pe, with R^2 values of 0.756 for experiments and 0.757 for simulations. It is interesting to note that the simulations consistently yield smaller trapping times relative to the experiments over the range of Pe probed. The 37% array appears to have a much steeper dependence on 1/Pe, and analysis of only the −80% and −8% overlap array data yields a better linear fit, with R^2 values of 0.936 and 0.972 for experiments and simulations, respectively. The reason for the stronger dependence on Pe in the 37% array is not known at this time. Consistent with the MD simulations of Kenward and Slater, no chain relaxation was seen during the final portion of the unhooking process in the BD simulations.[28] Because of the relatively low signal-to-noise ratio of the experimental imaging

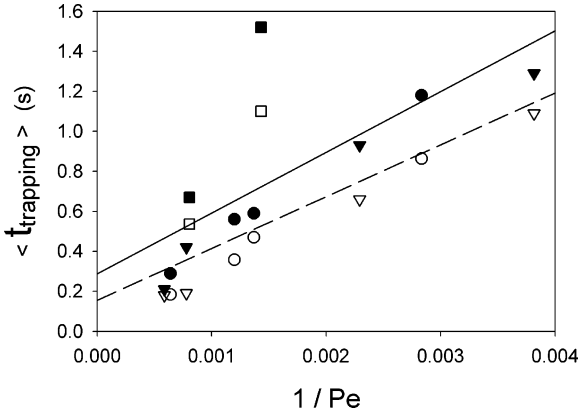

Figure 7. Experimental (closed symbols) and simulation (open symbols) results of mean unhooking time vs 1/Pe number at all overlap percentages and Pe listed in Table 1. Shapes of symbols indicate various overlap percentages: circles (−80%), triangles (−8%), and squares (37%). The solid line and dotted lines are linear fits to all the data for experiments and simulations, respectively. A minimum of 100 molecule ensembles were acquired for each experimental data point, and a minimum of 1000 chain ensembles were performed for each simulation point.

system, chain relaxation during unhooking could not be accurately investigated. To our knowledge, however, this is the first study in hydrodynamically driven flows in post arrays and provides compelling evidence regarding the ability of BD simulations to capture DNA dynamics in nontrivial flows.

Conclusions

Understanding the dynamics of biomolecules in complex flow is critical for the successful design of lab-on-a-chip devices. In this paper, we have demonstrated the first direct comparison of experiments and simulations of DNA transport in a complex pressure-driven flow. Because of recent interest in using post arrays to produce highly stretched DNA for on-chip sequencing applications,[19] we have focused on flow through ordered arrays. Qualitative and quantitative comparisons of experiments and Brownian dynamics simulations validate the simulations, which can be used to guide future designs.

The complex dynamics of DNA hooking and relaxation in a series of arrays were closely examined. Arrays that allowed little "channeling" led to most of the molecules hooking within the first 12 or so columns; e.g., at Pe = 262, in an array with −8% overlap, 72% of all molecules in the experiments and 95% in simulations were found to form at least one hook within the array. More significantly, both experiments and simulations demonstrate clearly that in an overlapping array configuration a considerable fraction of molecules undergo a hook within the first three columns for all Pe considered. Repeated hooks occur at specific distances downstream; however, because of relaxation within the array, little increase in fractional extension was observed in arrays longer than three columns. In general, long, multicolumn arrays cannot be easily optimized for producing fully or near fully stretched molecules: low flow strengths (or Pe) allow relaxation of the chains within longer arrays and high flow strengths reduce the molecule's collision cross section and result in the formation of few hooks after the initial one.

Hooking probabilities and DNA fractional extensions were also measured versus an initial impact parameter and support single post experiments showing that placement of DNA molecules near the stagnation streamline of posts increases the probability of hooking. The trapping time was found to scale as 1/Pe, indicating a "high field limit"; hence, these hydrodynamically trapped molecules display the same scaling for trapping as in electrophoresis, in agreement with the MD simulations and collision model of Kenward and Slater.[28]

Acknowledgment. This work was supported by NASA through Award NNC04GA72G. All microfabrication was performed in the Berkeley Microfabrication Laboratory. NPT acknowledges additional support through the University of California Mentored Research Fellowship and thanks Boris Stoeber and Sean Ferree for their invaluable assistance, Harvey Blanch for the use of experimental equipment, and Karen Webster, Cheok I. Cheong, and Andrew Lopez for experimental assistance.

References and Notes

(1) Schroeder, C. M.; Teixeira, R. E.; Shaqfeh, E. S. G.; Chu, S. *Macromolecules* **2005**, *38*, 1967−1978.
(2) Schroeder, C. M.; Shaqfeh, E. S. G.; Chu, S. *Macromolecules* **2004**, *37*, 9242−9256.
(3) Schroeder, C. M.; Babcock, H. P.; Shaqfeh, E. S. G.; Chu, S. *Science* **2003**, *301*, 1515−1519.
(4) Larson, R. G.; Hu, H.; Smith, D. E.; Chu, S. *J. Rheol.* **1999**, *43*, 267−304.
(5) Smith, D. E.; Chu, S. *Science* **1998**, *281*, 1335−1340.
(6) Perkins, T. T.; Smith, D. E.; Chu, S. *Science* **1997**, *276*, 2016−2021.
(7) Bakajin, O. B.; Duke, T. A. J.; Chou, C. F.; Chan, S. S.; Austin, R. H.; Cox, E. C. *Phys. Rev. Lett.* **1998**, *80*, 2737−2740.
(8) Jendrejack, R. M.; de Pablo, J. J.; Graham, M. D. *J. Chem. Phys.* **2002**, *116*, 7752−7759.
(9) Chen, Y. L.; Graham, M. D.; de Pablo, J. J.; Jo, K.; Schwartz, D. C. *Macromolecules* **2005**, *38*, 6680−6687.
(10) Hernandez-Ortiz, J. P.; de Pablo, J. J.; Graham, M. D. *J. Chem. Phys.* **2006**, *125*, 15.
(11) Chen, Y. L.; Graham, M. D.; de Pablo, J. J.; Randall, G. C.; Gupta, M.; Doyle, P. S. *Phys. Rev. E* **2004**, *70*, 4.
(12) Babcock, H. P.; Teixeira, R. E.; Hur, J. S.; Shaqfeh, E. S. G.; Chu, S. *Macromolecules* **2003**, *36*, 4544−4548.
(13) Shaqfeh, E. S. G.; McKinley, G. H.; Woo, N.; Nguyen, D. A.; Sridhar, T. *J. Rheol.* **2004**, *48*, 209−221.
(14) Doyle, P. S.; Shaqfeh, E. S. G.; McKinley, G. H.; Spiegelberg, S. H. *J. Non-Newtonian Fluid Mech.* **1998**, *76*, 79−110.
(15) Hsieh, C. C.; Li, L.; Larson, R. G. *J. Non-Newtonian Fluid Mech.* **2003**, *113*, 147−191.
(16) Jendrejack, R. M.; Schwartz, D. C.; de Pablo, J. J.; Graham, M. D. *J. Chem. Phys.* **2004**, *120*, 6315−6315.
(17) Jendrejack, R. M.; Schwartz, D. C.; de Pablo, J. J.; Graham, M. D. *J. Chem. Phys.* **2004**, *120*, 2513−2529.
(18) Jendrejack, R. M.; Schwartz, D. C.; Graham, M. D.; de Pablo, J. J. *J. Chem. Phys.* **2003**, *119*, 1165−1173.
(19) Chan, E. Y.; Goncalves, N. M.; Haeusler, R. A.; Hatch, A. J.; Larson, J. W.; Maletta, A. M.; Yantz, G. R.; Carstea, E. D.; Fuchs, M.; Wong, G. G.; Gullans, S. R.; Gilmanshin, R. *Genome Res.* **2004**, *14*, 1137−1146.
(20) Saville, P. M.; Sevick, E. M. *Macromolecules* **1999**, *32*, 892−899.
(21) Sevick, E. M.; Williams, D. R. M. *Phys. Rev. Lett.* **1996**, *76*, 2595−2598.
(22) Sevick, E. M.; Williams, D. R. M. *Phys. Rev. E* **1994**, *50*, R3357−R3360.
(23) Patel, P. D.; Shaqfeh, E. S. G. *J. Chem. Phys.* **2003**, *118*, 2941−2951.
(24) Andre, P.; Long, D.; Ajdari, A. *Eur. Phys. J. B* **1998**, *4*, 307−312.
(25) Randall, G. C.; Doyle, P. S. *Phys. Rev. Lett.* **2004**, *93*.
(26) Randall, G. C.; Doyle, P. S. *Macromolecules* **2005**, *38*, 2410−2418.
(27) Randall, G. C.; Doyle, P. S. *Macromolecules* **2006**, *39*, 7734−7745.
(28) Kenward, M.; Slater, G. W. *Eur. Phys. J. E* **2006**, *20*, 125−141.
(29) Deutsch, J. M. *Science* **1988**, *240*, 922−924.
(30) Deutsch, J. M.; Madden, T. L. *J. Chem. Phys.* **1989**, *90*, 2476−2485.
(31) Volkmuth, W. D.; Austin, R. H. *Nature (London)* **1992**, *358*, 600−602.
(32) Volkmuth, W. D.; Duke, T.; Wu, M. C.; Austin, R. H.; Szabo, A. *Phys. Rev. Lett.* **1994**, *72*, 2117−2120.
(33) Kaji, N.; Tezuka, Y.; Takamura, Y.; Ueda, M.; Nishimoto, T.; Nakanishi, H.; Horiike, Y.; Baba, Y. *Anal. Chem.* **2004**, *76*, 15−22.
(34) Doyle, P. S.; Bibette, J.; Bancaud, A.; Viovy, J. L. *Science* **2002**, *295*, 2237−2237.
(35) Minc, N.; Bokov, P.; Zeldovich, K. B.; Futterer, C.; Viovy, J. L.; Dorfman, K. D. *Electrophoresis* **2005**, *26*, 362−375.
(36) Minc, N.; Futterer, C.; Dorfman, K.; Bancaud, A.; Gosse, C.; Goubault, C.; Viovy, J. L. *Anal. Chem.* **2004**, *76*, 3770−3776.
(37) Long, D.; Ajdari, A. *Eur. Phys. J. E* **2001**, *4*, 29−32.

(38) Olson, D. J.; Johnson, J. M.; Patel, P. D.; Shaqfeh, E. S. G.; Boxer, S. G.; Fuller, G. G. *Langmuir* **2001**, *17*, 7396−7401.
(39) Beck, V. A. *Polymer Dynamics in Nonlinear and Microfluidic Flows*; Stanford University, Stanford, 2006.
(40) Smith, D. E.; Perkins, T. T.; Chu, S. *Macromolecules* **1996**, *29*, 1372−1373.
(41) Bustamante, C.; Marko, J. F.; Siggia, E. D.; Smith, S. *Science* **1994**, *265*, 1599−1600.
(42) Perkins, T. T.; Quake, S. R.; Smith, D. E.; Chu, S. *Science* **1994**, *264*, 822−826.
(43) Xia, Y. N.; Whitesides, G. M. *Annu. Rev. Mater. Sci.* **1998**, *28*, 153−184.
(44) Randall, G. C.; Doyle, P. S. *Proc. Natl. Acad. Sci. U.S.A.* **2005**, *102*, 10813−10818.
(45) Liu, T. W. *J. Chem. Phys.* **1989**, *90*, 5826−5842.
(46) Ottinger, H. C. *Stochastic Processes in Polymeric Fluids;* Springer: New York, 1996.
(47) Hur, J. S.; Shaqfeh, E. S. G.; Larson, R. G. *J. Rheol.* **2000**, *44*, 713−742.
(48) Shaqfeh, E. S. G. *J. Non-Newtonian Fluid Mech.* **2005**, *130*, 1−28.
(49) Vologodskii, A. *Macromolecules* **1994**, *27*, 5623−5625.
(50) Doyle, P. S.; Shaqfeh, E. S. G.; Gast, A. P. *J. Fluid Mech.* **1997**, *334*, 251−291.
(51) Russel, W. B.; Saville, D. A.; Schowalter, W. R. *Collodial Dispersions;* Cambridge University Press: New York, 1989.
(52) Ryckaert, J. P.; Ciccotti, G.; Berendsen, H. J. C. *J. Comput. Phys.* **1977**, *23*, 327−341.
(53) Song, L.; Maestre, M. F. *J. Biomol. Struct. Dyn.* **1991**, *9*, 87−99.

MA062892E